Journal of Applied Polymer Science

A Novel Method of Making PVF Porous Foam Without Using the Pore Forming Agent

You-Im Chang,[1] Wei-You Cheng,[1] Larry Jang[2]
[1]Department of Chemical Engineering, Tunghai University, Taichung, Taiwan 40704
[2]Department of Chemical Engineering, California State University, Long Beach, California 90840
Correspondence to: Y. I. Chang (E-mail: yichang@thu.edu.tw)

ABSTRACT: Different with the conventional method of manufacturing poly(vinyl formal) (PVF) porous foam by using the pore-forming agents such as wheat or potato starches, a novel method without using the pore-forming agent is introduced in this article. Through the help of images taken by a scanning electron microscope, the formation process of the present PVF foam will be discussed in terms of the spinodal decomposition (SD) phase separation principle. Additionally, the effect of poly(vinyl alcohol) concentration and reaction temperature on the pore structure of the PVF foam will be investigated. Moreover, the water adsorption capacities of the PVF foams obtained by the present method will be studied in details through the analyses of pore-size distribution, mechanical modulus, and thermal property. © 2014 Wiley Periodicals, Inc. J. Appl. Polym. Sci. **2015**, *132*, 41270.

KEYWORDS: foams; PVA superabsorbent; spinodal decomposition

Received 12 May 2014; accepted 29 June 2014
DOI: 10.1002/app.41270

INTRODUCTION

The porous poly(vinyl formal) (PVF) foam is a well-known superabsorbent polymer (SAP) made by poly(vinyl alcohol) (PVA), and can be used in cleaning and washing processes in either general household or electronic compartment manufacturing plants.[1] For example, PVF foam (a.k.a., "the super sponge") is commonly used to wash dishes, scrub kitchen, and bathroom sinks, dry the exteriors of automobiles, etc. In semiconductor manufacture plants, PVF foam can be made in the different types of sponge rollers used in the cleaning processes of hard disks and silicon wafers.[2] This PVF foam is characterized by its super water absorbent property, great durability and cleaning ability, and its super soft texture when moist. Using sulfuric acid as catalyst and a suitable pore-forming agent, this porous PVF foam was prepared through PVA and formaldehyde hybrid reaction (i.e., acetalization).

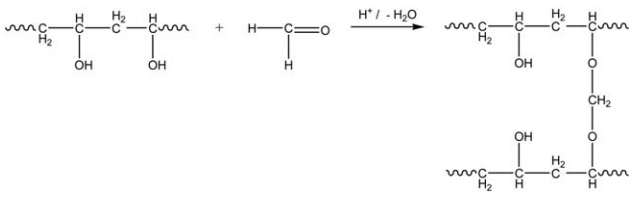

Large interconnected pores endow the PVF foam with unique spongy morphology and good resilience, both of which are controlled by the type of pore-forming agent employed. Owing to its complete biodegradability, starch is a pore-forming agent that has been commonly used in the making of porous PVF foam since 1960s.[3–6] It was reported that the average pore diameter of PVF foam varied from 30 to 60 μm when wheat-starch was used, and varied from 60 to 100 μm when potato-starch was used.[7,8] However, when those starch pore-forming agents were washed by water in the final step involved in manufacturing PVF foam, the high concentration of starch in the wastewater always caused serious environmental pollution problems because of its high COD value. In our previous article, we reported our efforts to reduce these high COD values by preparing PVF porous foam through the simultaneous acidification of water glass solution to produce silica particles as the pore-forming agent when PVF foam was made.[9] However, even with the benefits of low cost and low environmental impact, mixing those silica particles homogeneously with the PVA solution always proved difficult during the fabrication processes, due to the increased viscosity caused by the increased concentration of water glass solution.

Spinodal decomposition (SD) is essentially a mechanism for the rapid unmixing of a mixture of liquids (or solids) from one metastable phase (thermodynamically), to form two coexisting phases,[10] at which phase separation induced by chemical reaction to give various novel structural patterns of polymers have attracted considerable attention in last two decades.[11,12] When a polymer mixture is thermally quenched from a stable to

unstable regime at a constant temperature, one of the chief characteristics of a reaction-induced phase separation is that the quench depth changes with the reaction time. For example, when they investigated the phase separation problem of stilbene-labeled polystyrene/poly(vinyl methyl ether) (PSS/PVME) blends induced by irradiation with ultraviolet (UV) light, Ohta et al.[13] found that the photo-cross-linking reaction controls the time-evolution process of the SD in these binary polymer blends, and causes a drastic decrease in the mobility of the concentric domain structures with the progress of the reaction. When observing polymerization of *n*-butyl methacrylate (BMA) in the presence of poly(dimethylsiloxane-*co*-diphenylsiloxane), Wang et al.[14] found that there were three distinctive phase morphologies: moving droplets, networks, and sponge-like domains formed in the order of increasing initial BMA monomer weight fraction. The viscoelastic asymmetry was believed to play an important role in causing this phase separation in this reacting system. For synthesizing PVA hydrogels by repeated freeze/thawed cycles, Hassan and Peppas[15] found that, due to the phase separation mechanism, an increase in the number of freezing and thawing cycles reinforced the crystallinity and increased the densification of PVA gels. After studying the PVA gels formed in mixtures of dimethyl sulfoxide (DMSO) and water, Takeshita et al.[16] suggested that a SD type phase separation occurred in this system. The growth of the PVA domain network was extremely slowed down in the late phase separation stage because the elastic force of the gel suppressed the surface tension force, which was the driving force of domain growth. The shrinkage of PVA gel volume (syneresis) was caused by the relaxation process of the microscopic internal fluctuations produced at the end of the SD process. They also found that the growth kinetics of PVA gels was strongly dependent on the mixing ratio of DMSO and water in this gelation-induced phase separation system.[17]

In order to avoid the environmental pollution problem resulting from wastewater that contains high COD values caused by starch pore-forming agents and the mixing problem of silica particles that served as the pore-forming agent, a novel method of making PVF porous foam without using the pore forming agent is introduced in this article. Through the help of microscopic images recorded by a video camera, the formation process of the present PVF foam will be discussed in terms of the principle of SD phase separation. Additionally, the effect of PVA concentration and reaction temperature on the pore structure of the PVF foam will be investigated. Moreover, the water adsorption capacities of the PVF foams obtained by the present method will be studied in detail through analyses of pore-size distribution, mechanical modulus, and thermal property.

EXPERIMENTAL

Materials

Commercial PVA (BF-17; 99.3 wt %) with averaged polymerization degree of 1700 and hydrolysis degree of 98.5–99.2 mol % were obtained from Chang-Chun Petrochemical Co., Ltd, Taiwan. Deionized water was used for the solvent of PVA. Other reagents, which were all of analytical grade, were used as received.

PVF Foam Synthesis

A dispersion of 80 g PVA was first added to 380 mL of an aqueous solution heated to 95°C for 60 minutes in order to dissolve those PVA completely. The resulting mixture was poured into a 5-L double-layer glass reaction reactor equipped with a speed-controlled blender (IKA, T-25 digital, Germany) and a vacuum pump (ROCKER, Chemker-411, Taiwan), which was pre-heated to 50°C in a water-recirculating chiller (HSC, type 806, Taiwan). After mixing for 5 minutes as a speed of 10,000 rpm and 0.2 atm, 90 mL of 24 wt % formaldehyde solution and 30 mL of 50 wt % sulfuric acid was added, and the resulting mixture was mixed homogeneously for another 5 minutes while being stirred to obtain a reaction solution containing 12 wt % PVA. Other reaction solutions containing 13–16 wt % PVA were prepared by the same procedure.

Each of the above reaction solutions was finally introduced to a hard plastic rectangular vessel with a dimension of 15 cm × 20 cm and 5 cm in height. These vessels were then put in a temperature-controlled oven to carry out the acetalization reaction at 60°C for 8 hours. The resulting samples of porous PVF foam were washed thoroughly with water to remove the remaining sulfuric acid and formaldehyde. In order to investigate the effect of the reaction temperature, the PVF samples at the acetalization reaction for 12 hours at 50°C were also prepared by the same procedure.

Determination of the Conversion Rate of Formaldehyde

In order to determine the conversion rate of formaldehyde in the present acetalization reaction, the residual concentrations of formaldehyde in the reaction solutions at different reaction times were determined by the UV–Visible spectrophotometry.[18] According to this method, in the presence of excessive ammonium acetate (i.e. 15 g per 250 mL), the samples diluted with various amounts of distilled water were titrated by 2,4-pentanedione (i.e. 0.2 wt %) to form 3,5-diacetyl-1,4-hydrolutine, which is yellow in color and has a maximum absorbance of 412 nm.

Scanning Electron Microscope Imaging

To observe the pore-size distribution of the present PVF foams, the samples were coated with a thin layer of gold (coating at 5.0 Pa and 20 mA for 80 seconds) and then monitored by a scanning electron microscope (SEM, JSM-7000F, JEOL, Japan) at a 15 kV accelerating voltage.

Differential Scanning Calorimetry (DSC) and Thermogravimetric Analysis (TGA) Thermal Analyses

A Perkin-Elmer DSC Pyris-1 instrument was used to determine the glass transition temperature (T_g) of 5 mg of the present PVF foam samples. The temperatures were scanned from 0°C to 150°C with a heating rate of 20°C/min under nitrogen flow rate of 20 cm^3/min. The water adsorption capacity and the water desorption rate of PVF foams were determined using DuPont TGA-Q50 thermal analyzer.[19] Under nitrogen flow rate of 100 cm^3/min, the water adsorption capacity of PVF foams were calculated from the weight loss at 100°C when each 20 mg sample was heated from room temperature to 600°C with a heating rate of 10°C/min, and the water desorption rate was determined when each sample was heated at 50°C for 50 minutes, respectively.[9]

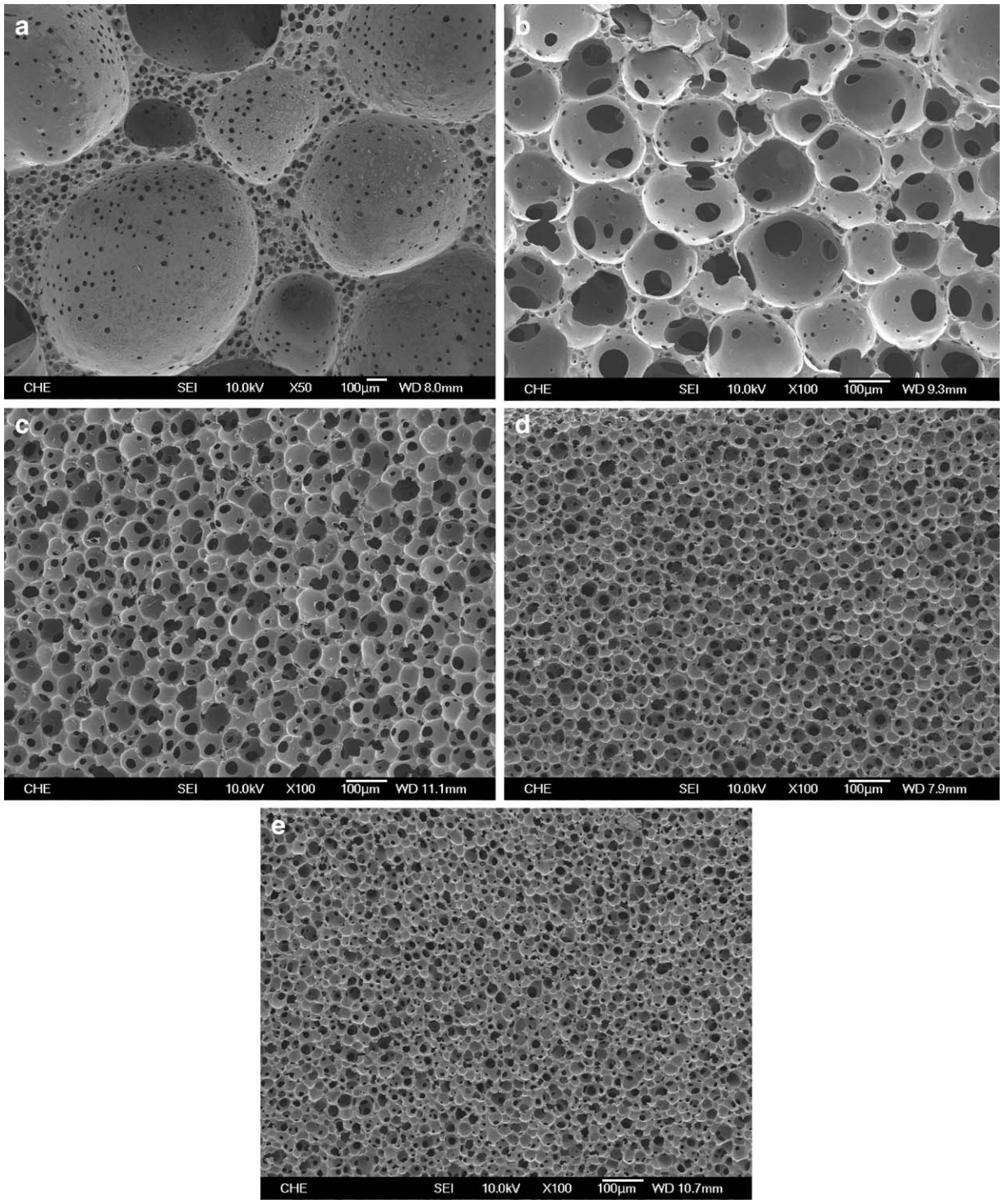

Figure 1. SEM pictures of the pore structure of PVF foams obtained in the present study, when various amounts 12 (**a**), 13 (**b**), 14 (**c**), 15 (**d**), and 16 wt % (**e**) of PVA reacted with 50 wt % sulfuric acid (i.e., acetalization reaction) for 12 hours at 50°C.

Tensile Test

An Instron Universal Test Machine (Model 4467) was adopted to measure the Young's modulus of PVF foams with 25 wt % water content according to the standard procedure described by ASTM D638-99. The cross-head load was 100*N* and the extending speed was 20 mm/min. The modulus values of the foam samples were determined by the average of six values.

RESULTS AND DISCUSSION

The Pore Structures of PVF Foams

Figures 1(a–e) and 2(a–e) show the SEM pictures of the pore structures of PVF foams, when various amounts (12, 13, 14, 15, and 16 wt %) of PVA reacted with 50 wt % sulfuric acid (i.e. acetalization reaction) for 12 hours at 50°C [see Figure 1(a–e)]

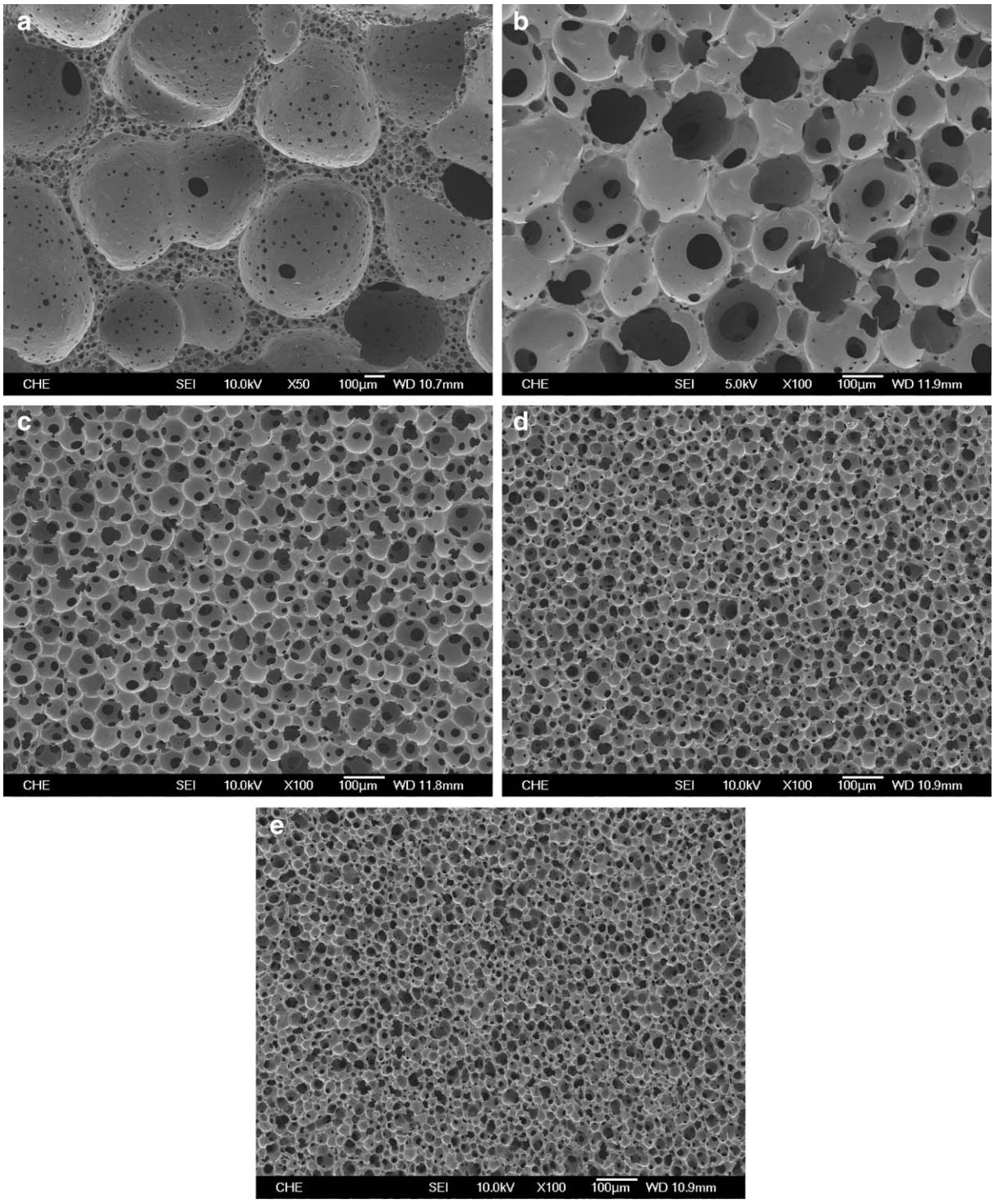

Figure 2. SEM pictures of the pore structure of PVF foams obtained in the present study, when various amounts 12 (**a**), 13 (**b**), 14 (**c**), 15 (**d**), and 16 wt % (**e**) of PVA reacted with 50 wt % sulfuric acid (i.e., acetalization reaction) for 8 hours at 60°C.

and 8 hours at 60°C [see Figure 2(a–e)], respectively. The pore structures of PVF foams shown in Figures 1(a–e) and 2(a–e) belong to a close-cell type, and the pore size decreases and the uniformity of pore size distribution increases with the increase of the PVA concentration when the reaction temperature is kept at either 50°C or 60°C. The average pore size is found to be as big as about 300 μm for 12 wt % PVA, but as small as about 30 μm for 16 wt % PVA for both of these two reaction temperatures. The increased solid content of PVA reactants is the major cause of this result; the higher the concentration of PVA, the smaller the pore size. By using the Image-Pro Plus software,[20] the measured porosities of PVF foams made at 50°C and 60°C

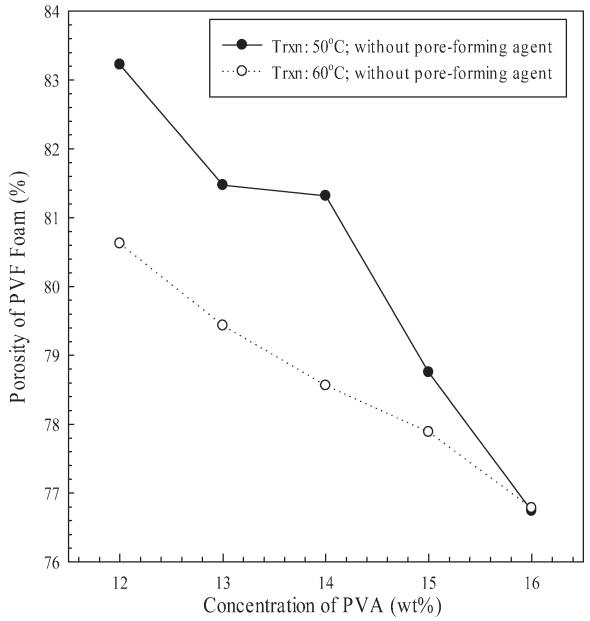

Figure 3. The measured porosities of PVF foams made at 50°C and 60°C analyzed by using the Image-Pro Plus software.[20]

are summarized in Figure 3. We found that the porosity of PVF foams made at 50°C can decrease from 83% to 77% when the PVA concentration increases from 12 to 16 wt %, and that the porosity of those PVF foams made at 60°C is always smaller than that of PVF foams made at 50°C. Two sets of the pore area analyzing examples of PVF foams are shown in Figure 4(a–d), respectively. For the PVF foams made by 12 wt % PVA, as shown in Figure 4(a, b), the intensity of large pore area (2×10^5 μm^2) made at 60°C is higher than those foams made at 50°C, which posses double intensity in small pore area of 10^5 μm^2. For 15 wt % PVA made PVF foams, as shown in Figure 4(c, d), the intensity distribution of pore area shift to the small area of 20 μm^2 as the reaction temperature is decreased from 60°C to 50°C. When the concentration of PVA is further increased to 16 wt %, as shown in Figure 4(e, f), these PVF foams made at these two temperatures attain the same intensity distribution of pore area. All these results coincide with the SEM observations of Figures 1(a–e) and 2(a–e): a higher porosity but smaller pore size foam can be obtained when the reaction temperature is decreased from 60°C to 50°C under the same PVA concentration. Interestingly, as can be observed in those SEM pictures, many micron voids exist on the pore walls of PVF foams made by either 12 and 13 wt % PVA (which are identical to those PVF pore walls when SiO_2 particles served as the pore-forming agent in our previous work[9]), but they disappear on the pore walls of those PVF foams made by 14–16 wt % PVA.

The results observed in the above SEM pictures of Figures 1(a–e) and 2(a–e) are due in large part to the increased rate of SD phase separation when the reaction temperature is increased from 50°C to 60°C under the same PVA concentration. As acetalization proceeds, since the affinity between PVF and H_2O molecules of aqueous solution decreases, many H_2O molecules become unbounded from the PVF and coalesce with those large water bubbles contained in the original PVA solution. The reaction rate increases as the reaction temperature increases, causing more H_2O molecules to become unbounded. Consequently, larger water bubbles can be formatted at 60°C than that at 50°C. Also, this SD phenomenon can be accelerated by the decreased viscosity of the PVA reaction solution when the reaction temperature is increased from 50°C to 60°C. Since the viscosity of the PVA reaction solution adopted in the present experiments increases with the increase of either PVA concentration or the decrease of solution temperature,[9] as illustrated by the schematic diagram in Figure 5, because of its decreased viscosity, the drainage velocity of the PVF polymer formatted at 60°C between two water bubbles is faster than that of 50°C under the same PVA concentration. This increased drainage velocity reduces the wall thickness of PVF formatted between two water bubbles, and therefore can easily induce a larger pore size in PVF foams at 60°C than that at 50°C.

The Conversion Rate of Formaldehyde

By taking 13 wt % PVA made PVF foams as an illustrated example, the time-dependent conversion rates of formaldehyde at 50°C and 60°C are shown in Figure 6. This figure demonstrates that the conversion rate of formaldehyde increases with the increase of reaction time, and that the values obtained at 60°C are always higher than those values at 50°C. For the reaction temperature at 60°C, a conversion rate of 57% can be obtained at the eighth hour, beyond which the conversion rate of formaldehyde approaches a constant value. When the reaction temperature decreases to 50°C, a conversion rate of 56% can be obtained at the twelfth hour for the present PVF sample. For the reaction temperature at 60°C when the reaction time was extended to 9 hours or longer, we found that the volume of the PVF sample starts to shrink (syneresis) because of the increased surface-induced shrinkage stress caused by the self-linkage between those unreacted hydroxyl groups located in the interior of PVA chains (which will therefore decrease effective cross-linking reaction between PVA and formaldehyde molecules).[21] This same volume shrinkage phenomenon was observed for those PVF samples obtained at the reaction temperature of 50°C when their reaction times were beyond 12 hours. Based on this result, a reaction time of 8 hours and of 12 hours was therefore chosen for the reaction temperature of 60°C and of 50°C in the present experiments, respectively.

The Microscopic Images Recorded by Video Camera

The SD phase separation morphology of making PVF foam by 13 wt % PVA at 60°C can be evidenced by the microscopic images taken by a video camera of reaction times of 0.5 [Figure 7(a)], 15 [Figure 7(b)], 18 [Figure 7(c)], 21 [Figure 7(d)], 24 [Figure 7(e)], and 30 minutes [Figure 7(f)]. As illustrated in Figure 7(a–f), the time-evolution process can be divided into three stages. At the first stage, as shown by Figure 7(a), when the first spinodal decomposition phenomenon occurred after reaction of 0.5 minutes, we observe the nematic nucleation of the PVF domains and many small water bubbles (i.e., condensed from acetalization) appear simultaneously as the PVA monomers react to form PVF polymers. As the additional acetalization continues, the nematic domains continue to nucleate

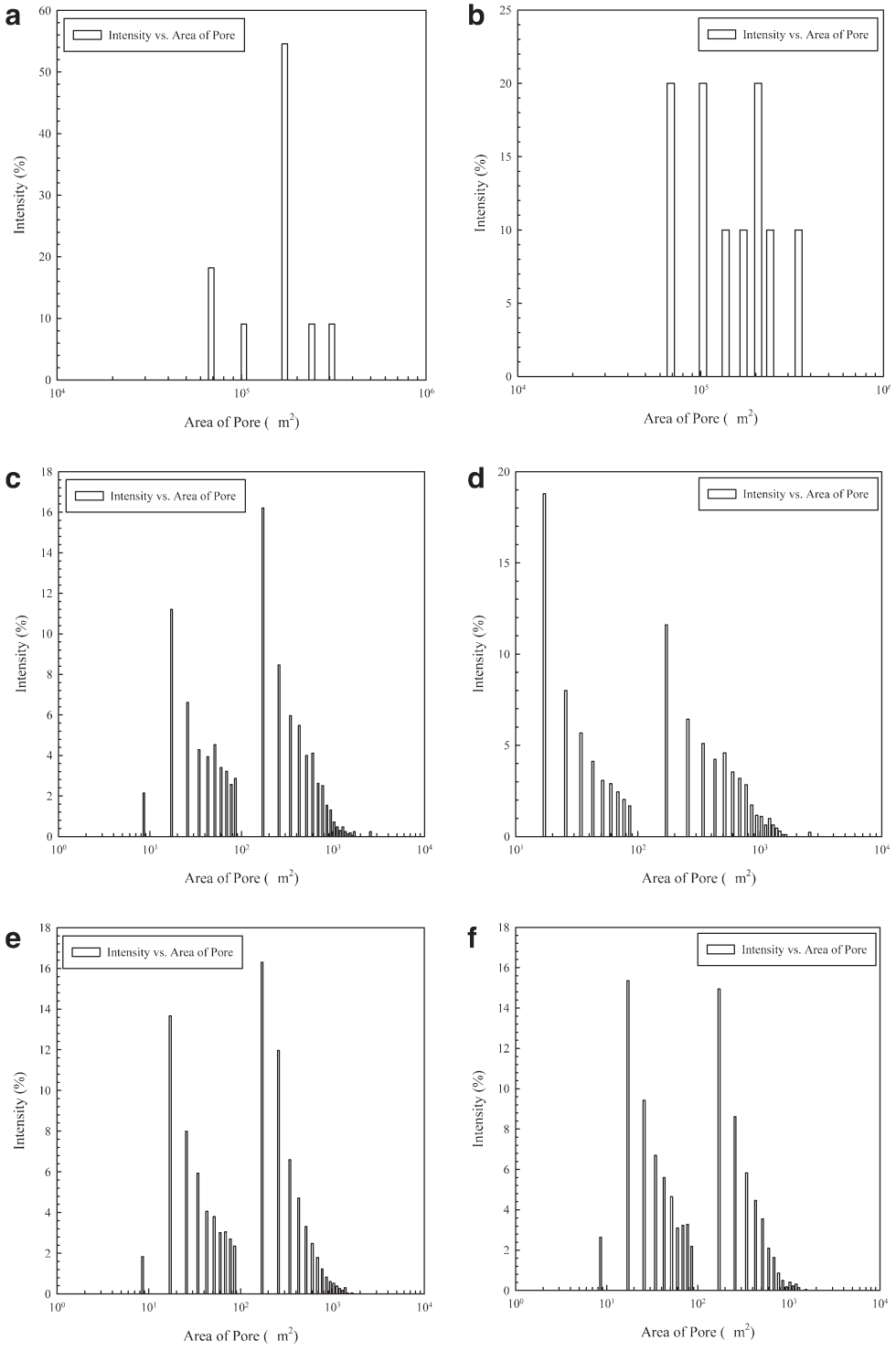

Figure 4. The pore area distribution of PVF foams analyzed by using the Image-Pro Plus software,[20] when PVF foams made by various amounts of PVA at either 50°C or 60°C. (**a**) 12 wt % PVA at 60°C; (**b**) 12 wt % PVA at 50°C; (**c**) 15 wt % PVA at 60°C; (**d**) 15 wt % PVA at 50°C; (**e**) 16 wt % PVA at 60°C; (**f**) 16 wt % PVA at 50°C.

and the small water bubbles start to separate from the PVF nucleates. Those micron voids that exist on the pore walls of PVF foams made by 12 and 13 wt % PVA [see Figures 1(a, b) and 2(a, b)] are believed to be formed by condensed water at this stage.[9] At the second stage of the reaction, as shown by Figure 7(b) after reaction of 15 minutes (i.e., when the conversion rate of formaldehyde achieves 20%; see Figure 6), since the large free energy barrier between small water bubbles is already

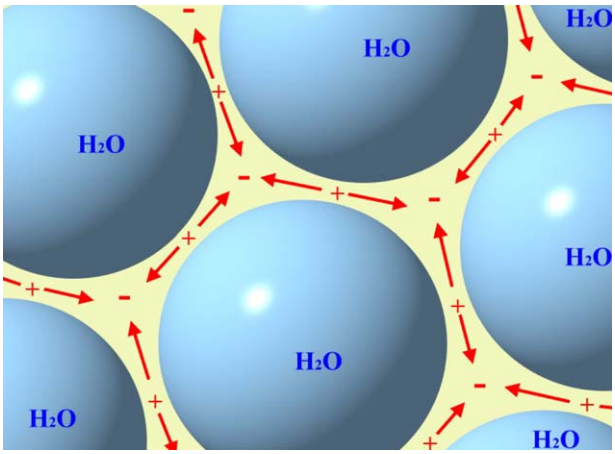

Figure 5. The schematic diagram describing the drainage phenomenon of the PVF polymer formatted between two water bubbles (i.e., the pore wall thickness of PVF foams). The capillary pressure difference between PVF polymer and plateau borders (i.e., at positions of inter-film contact) leads to rapid PVF wall thinning (over pressure is indicated by +, low pressure by −). [Color figure can be viewed in the online issue, which is available at wileyonlinelibrary.com.]

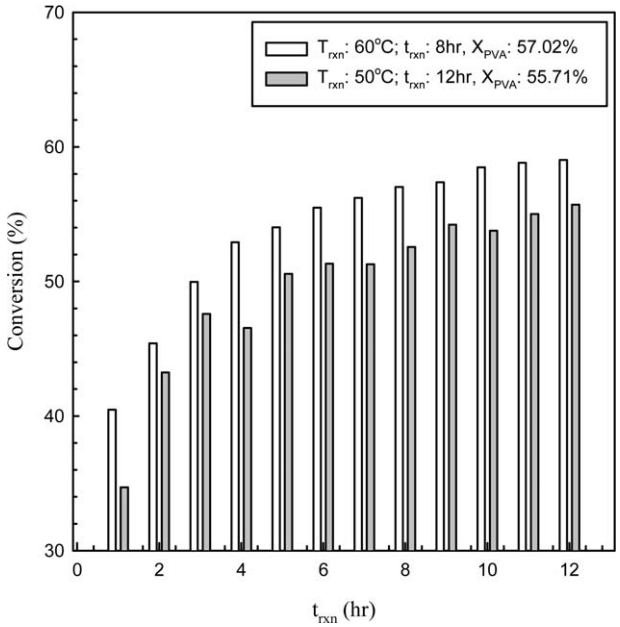

Figure 6. The time-dependent conversion rates of formaldehyde for PVF foams made by 13 wt % PVA at 50°C and 60°C, respectively.

overcome, we observe fast movement of small condensed water molecules followed by rapid coalescence with large water bubbles contained in the original PVA solution, and the drainage of PVF polymers between two water bubbles. At the third reaction stage, as shown by Figure 7(f) after reaction of 30 minutes (i.e., when the conversion rate of formaldehyde achieves 50%; see Figure 6), the speed of both SD phase separation and drainage phenomena become slow, and the PVF polymer matrix has grown sufficiently in molecular weight. The resulting morphology consists of water bubbles dispersed homogenously in a sponge-like polymer matrix whose water pore size decreases as the reaction temperature decreases from 60°C to 50°C.

Phase Diagram

The above SD phase separation can be illustrated on a ternary phase diagram exhibiting a miscibility gap. In this diagram, phase separation occurs whenever a mixture transitions into the

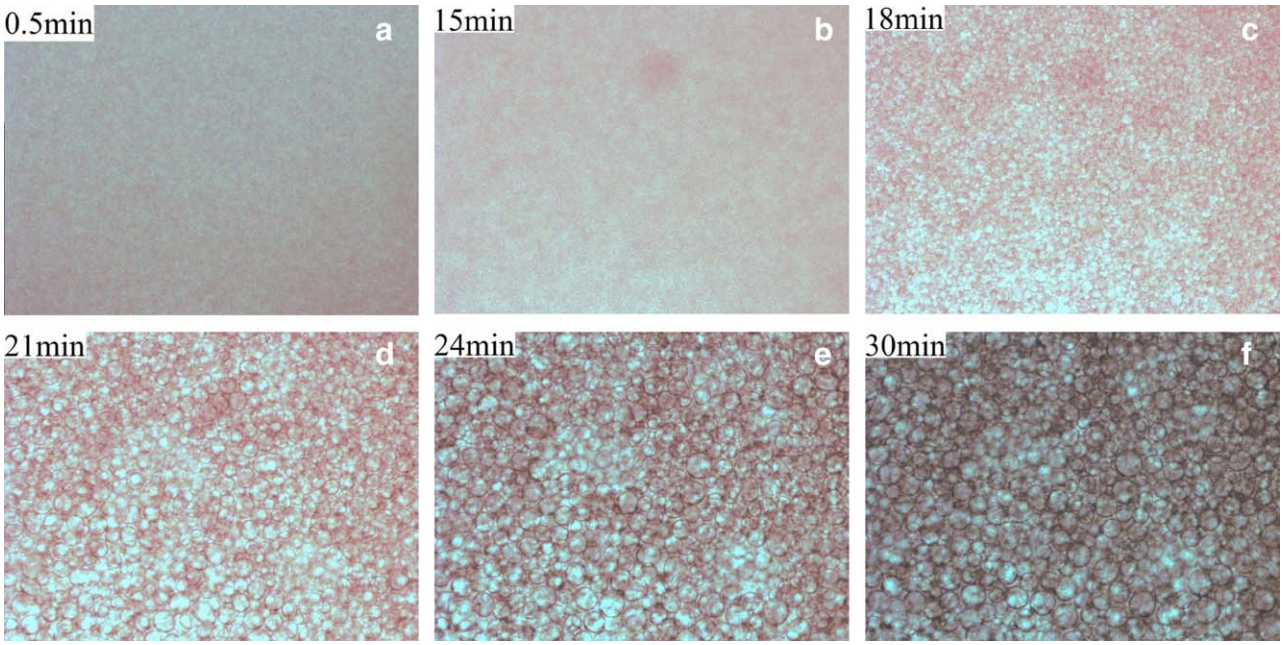

Figure 7. The SD phase separation morphology of the present acetalization evidenced by the microscopic images taken by a video camera recorded on the videotape at various reaction times of 0.5 (**a**), 15 (**b**), 18 (**c**), 21 (**d**), 24 (**e**), and 30 minutes (**f**). [Color figure can be viewed in the online issue, which is available at wileyonlinelibrary.com.]

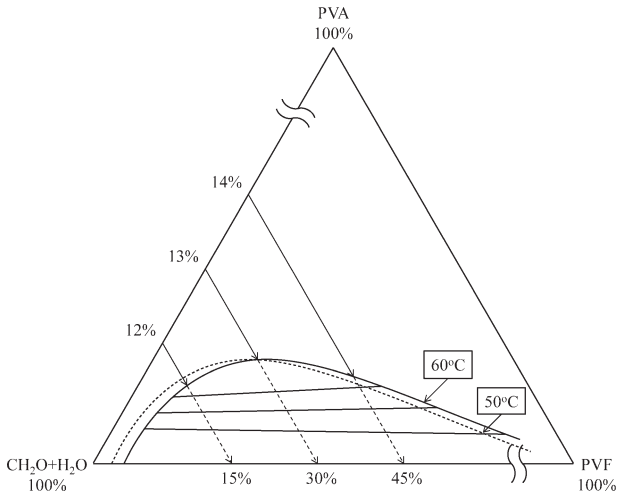

Figure 8. Schematic phase diagram of acetalization reaction induced SD phase separation in the PVA/PVF/$CH_2O + H_2O$ (i.e., formaldehyde solution) system.

unstable region of this miscibility gap (i.e., the spinodal region), whose boundary is referred to as the binodal or coexistence curve. Based on the time-dependent conversion rates of formaldehyde obtained in Figure 6 and the above microscopic recorded images obtained for those PVF foams made by 12–16 wt % PVA, a speculated rough sketch of the phase diagram of the PVA/PVF/$CH_2O + H_2O$ (i.e., formaldehyde solution) system is shown in Figure 8. As acetalization reaction proceeds, the composition of the reaction mixture changes along a straight line (e.g., when PVA = 13 wt % reacts at 60°C) parallel to the side connecting the vertexes of the monomer PVA and its product polymer PVF. The SD phase separation is caused by segregation between PVF and $CH_2O + H_2O$ phases, and thus the phase boundary has a dome shape as shown in Figure 8. In the case of PVA = 12 wt % reacts at 60°C, the acetalization reaction path intersects with the coexistence curve on the PVF-poor side. The reaction proceeds rapidly at the beginning period, where the nematic nucleation of the PVF domains and many small water bubbles [i.e., condensed from acetalization; see Figure 2(a)] appear simultaneously. When the path crosses over the coexistence curve and gets into the two-phase region, the reaction gradually becomes slow as PVA is consumed. However, in the case of PVA = 13 wt % reacted at 60°C, the reaction path will intersect with the coexistence curve at a point of the PVF-rich side which is close to the top of the dome as shown in Figure 8. When the reaction path crosses over this point and gets into the two-phase region as the additional acetalization continues, and the nematic domains of PVF continue to nucleate and the small water bubbles start to separate from the PVF nucleates as shown by the second stage of the reaction of Figure 7(b), the rapid coalescence of small condensed water molecules with those large water bubbles and the drainage of PVF polymers between two water bubbles (see Figure 5) will cause the SD phase separation to occur consequently. When the concentration of PVA is further increased from 13 to 14 wt %, the total volume of the PVF-rich phase increases with proceeding of the acetalization reaction and eventually those large water bubbles will disconnect with each other, turning the PVF-rich phase into a sponge-like PVF polymer matrix as shown in Figures 1(c) and 2(c). The coexistence curve of PVF and condensed H_2O phases for the reaction temperature of 50°C is also shown by the dashed lines in the Figure 8. Because of the smaller reaction rate at the same PVA concentration, its dome-shape like curve shifts to the left hand side of the curve of 60°C, and therefore a higher PVA concentration is required to cause SD phase separation than that of 60°C.

Young's Modulus of PVF Foams

Figure 9 shows the Young's modulus of PVF foams made by 12–16 wt % PVA at the eighth and twelfth hour of reaction time when the reaction temperature is kept at 60°C and 50°C, respectively. In this figure, we can find that the higher the concentration of PVA, the larger the Young's modulus of PVF foams in general, except that there is a minimum existed at 13 wt % PVA when the reaction temperature is kept at 50°C. This existence of this minimum modulus at 50°C is probably caused by the fact that the viscosity of those PVF foams made by 12 wt % PVA is low enough to increase the drainage velocity of PVF polymers as shown in Figure 5, and therefore increase the mass content of PVF in the plateau borders of the polymer matrix (i.e., the regions of interfilm contact as shown in Figure 5), which increases the entanglement of PVF chains in this border region and gives their final foams larger modulus than those PVF foams made by 13 wt % PVA at 50°C as shown in Figure 9. Also, because the PVF foams made at 50°C always posses higher porosity but smaller pore size caused by the smaller drainage velocity of PVF polymer as shown in Figure 5, which makes their pore walls thicker than those foams made at 60°C, the foam's modulus made at 50°C is higher than that made at 60°C.

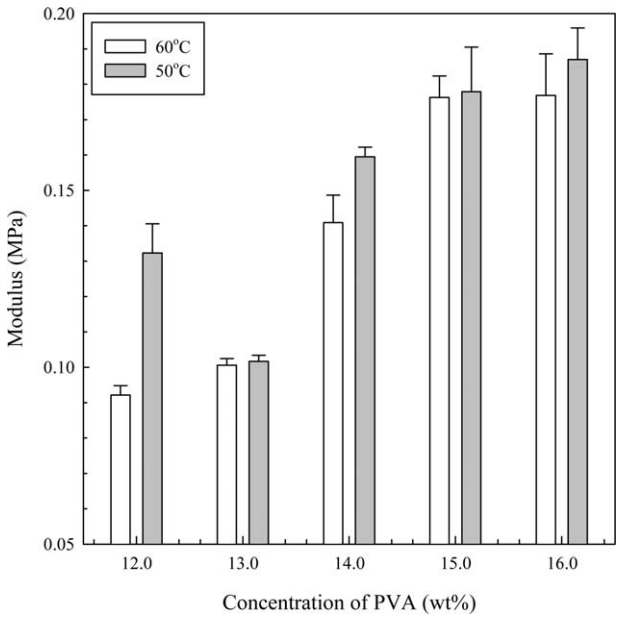

Figure 9. The Young's modulus of PVF foams made by 12–16 wt % PVA at the eighth and twelfth hour of reaction time when the reaction temperature is kept at 60°C and 50°C, respectively.

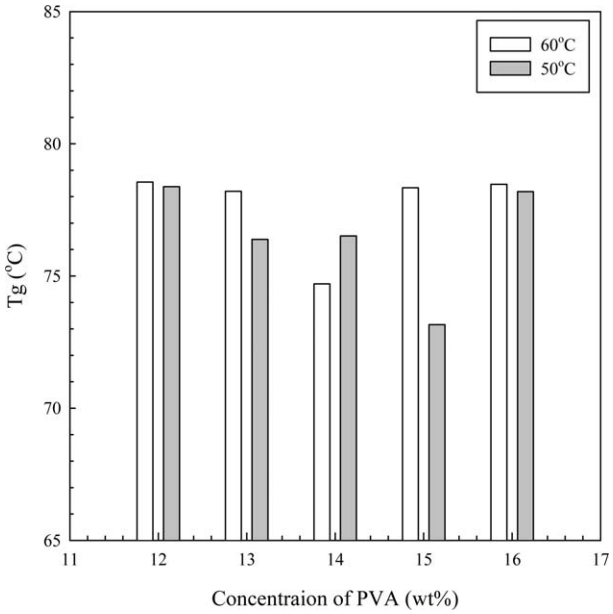

Figure 10. The glass transition temperature T_g of PVF foams made by 12–16 wt % PVA at the eighth and twelfth hour of reaction time when the reaction temperature is kept at 60°C and 50°C, respectively.

Glass Transition Temperature T_g of PVF Foams

As shown in Figure 10 for all ranges of PVA concentrations adopted in the present experiments, because of the stronger cross-linking polymer chain formation caused by the higher conversion rate at 60°C, the T_g of PVF foams made at this temperature is higher than those foams made at 50°C. A minimum T_g is observed to locate at 15 wt % PVA when the reaction temperature is kept at 50°C, while to locate at 14 wt % PVA for 60°C reaction. The increased crystalline state (see Chapter 6 in Sperling's textbook[11]) caused by the increased entanglements of PVF chains in the plateau borders shown in Figure 5 can be applied to explain why the PVFs' T_g made by 13 wt % PVA at 60°C and by 14 wt % PVA at 50°C are higher than those T_g made by 14 wt % PVA at 60°C and by 15 wt % PVA at 50°C, respectively.

Water Adsorption Capacity and Water Desorption Rate of PVF Foams

To behave as an SAP, since the water adsorption capacity of PVF foam is one of the most import properties needed to be identified, therefore we have tested it as follows.

The water adsorption capacity of the water saturated PVF foams can be determined from the TGA curves of sample weight loss at 100°C,[9] and Figure 11 summarizes the water adsorption capacity of the present PVF foams made by 12–16 wt % PVA at 50°C and 60°C, respectively. Their water adsorption capacities of 82%–87% all meet the requirement of SAP.[1] Also, we can find that the higher the mass content of PVA, the lower the water adsorption capacity of the PVF foams. However, as shown in Figure 11, we also find that the equality between the water adsorption capacity obtained by the above TGA method and the theoretical value is achieved only for the 13 wt % PVA made PVF foam at 60°C, and all other samples' water adsorption capacities are smaller than their theoretical values. These inequalities are arisen by the following two facts: (1) When PVA concentration is smaller than 13 wt %, the faster drainage velocity drives more PVF polymers to reseat in the regions of plateau borders and therefore reduces the uniformity of pore size distribution. (2) When PVA concentration is greater than 13 wt %, the volume shrinkage caused by the over self-linkage reaction happened in the interior of PVA chains. In order to explain why that the water adsorption capacities of those PVF foams made at 60°C are higher than those foams made at 50°C as shown in Figure 11, we have conducted the analyses of bound water and free water in details as follows.[19]

The free water content of a water saturated PVF foam can be determined by using DSC; that is, the PVF sample was frozen within the instrument to −30°C and heated to 30°C with a scanning rate of 5°C/min, then its free water content can be determined from the transition enthalpy for the melting of frozen water, which formats the majority of those water molecules absorbed by the PVF foams. Figure 12 shows a representative DSC curve obtained by using this method for the 13 wt % PVA foam made at 60°C. By deducting this free water content from the value of the above water adsorption capacity, the bound water content of PVF foams can then be determined; that is, the bound water defined in the present article is the water molecules combined with those unreacted hydroxyl groups located in the interior of PVA chains. The analysis results of the contents of free water and bound water for those PVF foams made at 50°C and 60°C are summarized at Figure 13(a, b), respectively. Because of their larger porosity (see Figure 3), the free water contents for the PVF foams made at 50°C are higher than those foams made at 60°C, but the opposite is true for the bound water contents. Due to the higher conversion rate of

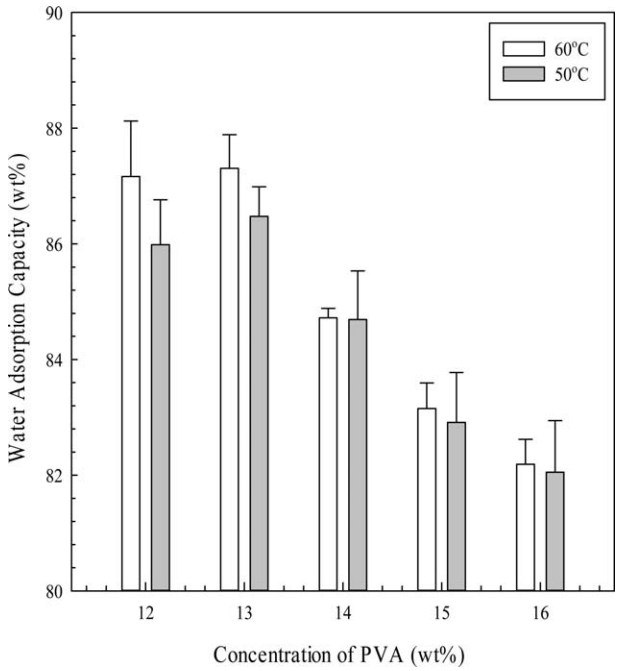

Figure 11. The water adsorption capacities of the PVF foams made by 12–16 wt % PVA at 50°C and 60°C, respectively.

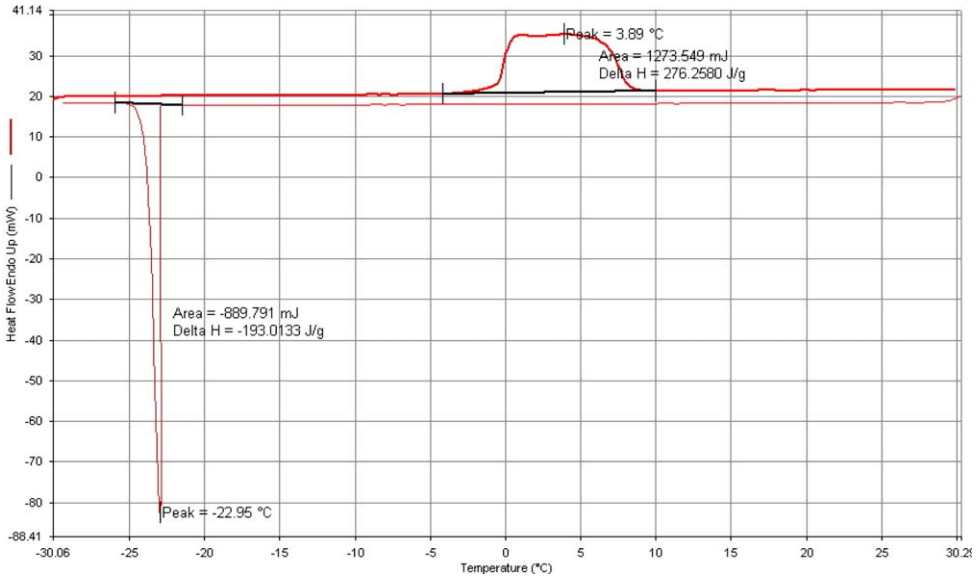

Figure 12. The representative DSC curve used to determine the free water content of the 13 wt % PVA foam made at 60°C. [Color figure can be viewed in the online issue, which is available at wileyonlinelibrary.com.]

formaldehyde obtained at 60°C (see Figure 7), which increases the difficulty for those water molecules to penetrate into the interiors of the PVA chains and to combine with those unreacted hydroxyl groups, and therefore those PVF foams made at 60°C always own less bound water than those PVF foams made at 50°C. Also, because the 14 wt % PVA made foam owns the highest pore size uniformity and the lowest volume shrinkage at either 50°C or 60°C, so its free water content is the highest (therefore the bound water content is the lowest) among those foams made by 12–16 wt % PVA in the present article.

The water desorption rates of the PVF foams can be determined from the slopes of the water retention curves as shown in Figure 14(a, b), which were obtained by heating the PVF samples in TGA at 50°C for 50 minutes.[9] From the slopes of those water retention curves, because the 14 wt % PVA made foams own the highest pore size uniformity and the lowest volume shrinkage, so their water desorption rates are the highest among those foams made at either 50°C or 60°C. Because of their lager porosity, so the water desorption rates of those foams made at 50°C are slightly higher than those foams made at 60°C.

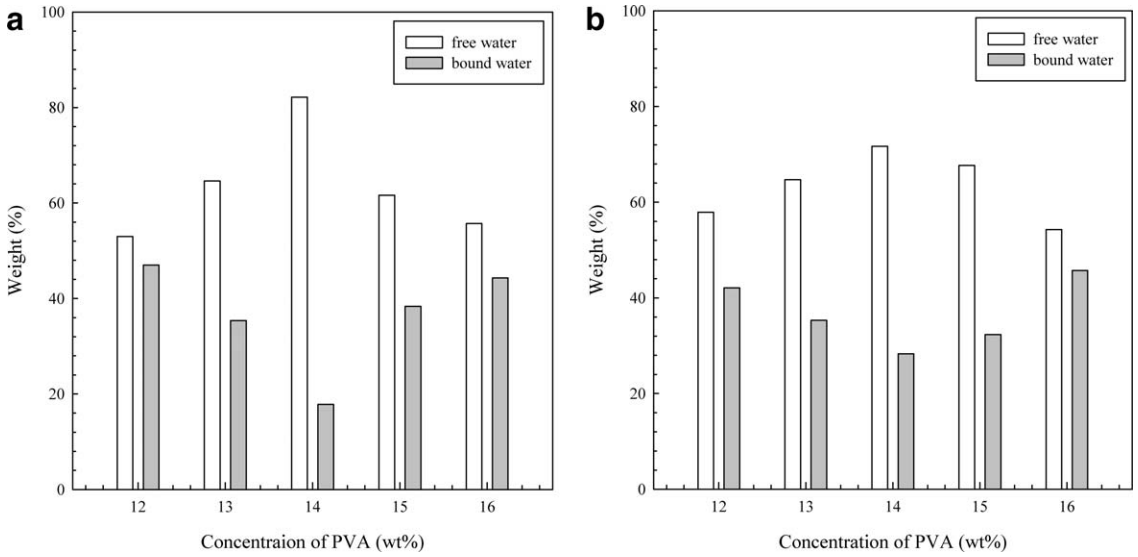

Figure 13. The analysis results of the contents of free water and bound water for the PVF foams made by 12–16 wt % PVA at 50°C (**a**) and 60°C (**b**), respectively.

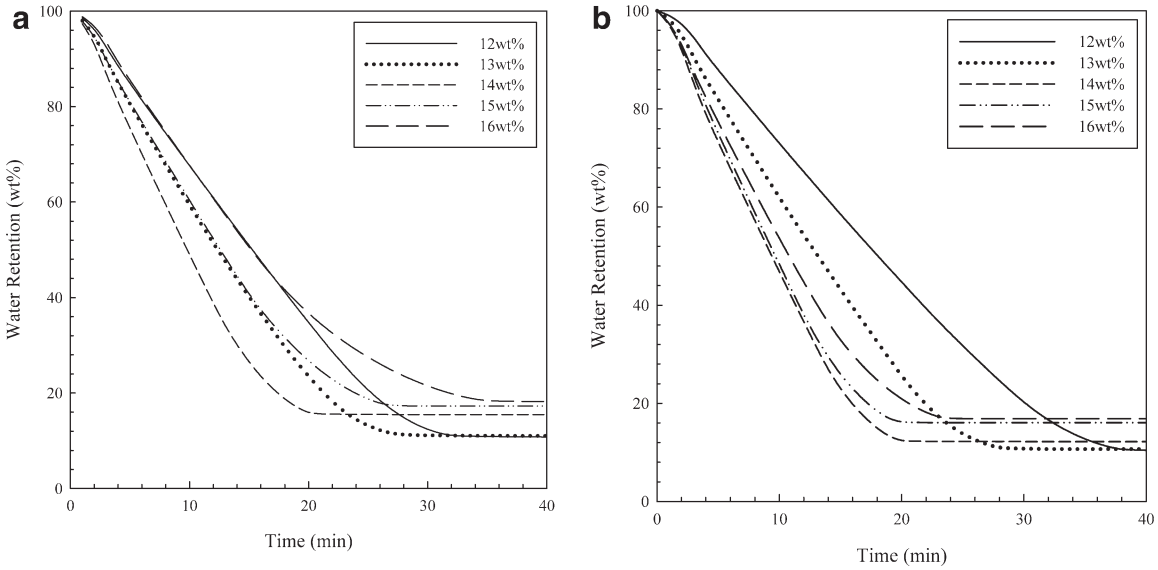

Figure 14. The water retention curves for the PVF foams made by 12–16 wt % PVA at 50°C (**a**) and 60°C (**b**), when the PVF samples were heated at 50°C in TGA for 50 minutes, respectively.

CONCLUSION

In order to avoid the problems of environmental pollution and mixing difficulty caused by those pore-forming agents such as wheat starches and silica particles, a novel method of fabricating porous PVF foams without using the pore forming agent is presented in this study. After conducting our analyses with the help of SEM, DSC, TGA, and stress–strain data, we have arrived at seven conclusions: (1) The pore structures of the present PVF foams belong to a close-cell type, and the pore size decreases and the uniformity of pore size distribution increases with the increase of the PVA concentration when the reaction temperature is kept at either 50°C or 60°C. (2) Under the same PVA concentration, because of the increased rate of SD phase separation and the increased drainage velocity of PVF polymers which can reduce the pore wall thickness, the PVF foams made at 60°C own a smaller porosity but larger pore size than those foams made at 50°C. (3) For the 13 wt % PVA made PVF foams, we find that both the conversion rate of formaldehyde and Young's modulus of PVF samples increase with the increase of reaction time, and both values obtained at 60°C are always higher than those values at 50°C. (4) In addition to the Young's modulus of PVF foams increases with the increase of PVA concentration in general, we find that the foam's modulus made at 50°C is higher than that made at 60°C. (5) Because of the stronger cross-linking polymer chain formation caused by the higher conversion rate at 60°C, the T_g of PVF foams made at this temperature is higher than those foams obtained at 50°C. (6) The water contents of those PVF foams made at 60°C are higher than those foams made at 50°C, and this result can be explained through the bound water and free water analyses. (7) Because of its highest pore size uniformity and lowest volume shrinkage, the 14 wt % PVA made foam made at either 50°C or 60°C owns the highest free water (therefore the bound water content is the lowest) and the highest water desorption rate among those PVA concentrations of 12–16 wt % adopted in the present article.

ACKNOWLEDGMENTS

The financial support received from the National Science Council of the Republic of China, research grant no. NSC 99-2221-E-029-021-MY3, is greatly appreciated.

REFERENCES

1. Buchhlz, F. L.; Graham, T. Modern Superabsorbent Polymer Technology; Wiley-VCH: New York, **1998**.
2. Zhang, F.; Busnaina, A. A.; Ahmadi, G. *J. Electrochem. Soc.* **1999**, *146*, 2665.
3. Wilson, C. L. US Pat. 2,609,347, **1952**.
4. Kern, W.; Schulz, R. C.; Braun, D. *J. Polym. Sci.* **1960**, *48*, 91.
5. Nishimura, H.; Sata, S. US Pat. 3,663,470, **1972**.
6. Sueoka, A.; Okamoto, T.; Ohmori, A.; Kawai, S.; Ueda, M. US Pat. 4,279,752, **1981**.
7. BeMiller, J. N.; Whistler, R. L. Starch: Chemistry and Technology, 3rd ed.; Academic Press: New York, **2009**.
8. Wilson, J. D.; Bechtel, D. B.; Todd, T. C.; Seib, P. A. *Cereal Chem.* **2006**, *83*, 259.
9. Chang, Y. I.; Cheng, W. Y.; Jang, L. *J. Appl. Polym. Sci.* **2014**, *131*, 39894.
10. Cahn, J. W. *Trans. Met. Soc. AIME* **1968**, *242*, 168.
11. Sperling, L. H. Introduction to Physical Polymer Science, 4th ed.; John Wiley & Sons: Hoboken, New Jersey, **2006**; Chapter 4.
12. Silverstein, M. S. *Polymer* **2014**, *55*, 304.
13. Ohta, T.; Urakawa, O.; Tran-Cong, Q. *Macromolecules* **1998**, *31*, 6845.

14. Wang, X.; Okada, M.; Han, C. C. *Macromolecules* **2006**, *39*, 5127.

15. Hassan, C. M.; Peppas, N. A. *Macromolecules* **2000**, *33*, 2472.

16. Takeshita, H.; Kanaya, T.; Nishida, K.; Kaji, K. *Macromolecules* **2001**, *34*, 7894.

17. Takahashi, N.; Kanaya, T.; Nishida, K.; Kaji, K. *Macromolecules* **2007**, *40*, 8750.

18. *Standard method No. JIS-L-1041:2011*, listed at JSA web store of http://www.jsa.or.jp/, Japanese Standards Association, 2011.

19. Plieva, F. M.; Karlsson, M.; Aguilar, M. R.; Gomez, D.; Mikhalvosky, S.; Galaev, I. Y.; Mattiasson, B. *J. Appl. Polym. Sci.* **2006**, *100*, 1057.

20. *Image-Pro Plus version 4.5*; Media Cybernetics Inc.: Bethesda, Maryland, **2001**.

21. Nephew, J. B.; Nihei, T. C.; Carter, S. A. *Phys. Rev. Lett.* **1998**, *80*, 3276.